Lee *et al. Terrestrial, Atmospheric and Oceanic Sciences* (2025) 36:11
https://doi.org/10.1007/s44195-025-00090-0

Terrestrial, Atmospheric and Oceanic Sciences

RESEARCH Open Access

Fast report: surface deformation associated with the 2025 Dapu earthquake

Zixin Lee[1], Ray Y. Chuang[1*], I-Ting Wang[1], Lishiue Chen[1], Wu-Lung Chang[2], Chi-Yu Chiu[2], Kuo-En Ching[3], Sheng-Wei Guo[1] and Chien-Liang Chen[4]

Abstract
On January 20th of 2025, a M6.4 earthquake struck the Dapu area in southwestern Taiwan. The event caused damage in Chiayi County and Tainan City, particularly in Nanxi District, where surface deformation was anticipated. In response, we conducted a rapid geodetic survey to investigate coseismic displacement fields from GNSS and InSAR observations. The result indicates surface displacements of up to several centimeters without visible interferogram discontinuity. To assess the fault slip, we applied a half-space dislocation model to evaluate two possible fault planes: a west-dipping and an east-dipping fault, both derived from the AutoBATS focal mechanism. Additionally, we analyzed pre-seismic surface deformation by using GNSS and InSAR time series data. Our findings reveal a high shortening rate (> 35 mm/yr) across the western foothills at this latitude without an obvious velocity gradient around the epicenter. These results enhance our understanding of the fault dynamics in southwestern Taiwan and highlight the critical role of geodetic data in seismic hazard assessments.

Keywords DInSAR, Coseismic displacements, Dislocation model, Slip inversion

1 Introduction

The M6.4 Dapu earthquake struck the Dapu area of Chiayi, southwestern Taiwan, on January 20, 2025. This event impacted Chiayi County and Tainan City, with the highest shaking observed in the Nanxi and Yujing districts of Tainan City (Wu et al. 2025). A few buildings and roads near the epicenter were damaged (Ou et al. 2025). The real-time fault plane solution from the Auto Broadband Array in Taiwan for Seismology (AutoBATS) (Jian et al. 2018) (https://tecdc.earth.sinica.edu.tw/FM/AutoBATS/) identified the mainshock as a thrust-faulting event with a strike oriented approximately SSW-NNE with a moment magnitude (Mw) 6.04 and a depth of ~ 10 km.

According to the active fault map from the Taiwan Geological Survey and Mining Management Agency (GSMMA), several active faults are near the epicenter, including the Koushiaoli and Tsochen faults, which are located west of the epicenter. This region surrounding the epicenter primarily consists of Yunshuichi Formation and Chunlun Formation (Lin and Chen 2016). The earthquake occurred at the depth of ~ 10 km, likely below the detachment in this region (e.g., Yang et al. 2010; Le Béon et al. 2024). While a deeper structure has been proposed in this area (Mouthereau et al. 2001), the depth of this event suggests that the earthquake may occur on a less well-understood structure. To analyze the surface deformation associated with the earthquake, we processed geodetic data including Global Navigation Satellite System (GNSS) and interferometric synthetic aperture radar

*Correspondence:
Ray Y. Chuang
raychuang@ntu.edu.tw
[1]Department of Geography, National Taiwan University, Taipei, Taiwan
[2]Department of Earth Sciences, National Central University, Taoyuan, Taiwan
[3]Department of Geomatics, National Cheng Kung University, Tainan, Taiwan
[4]Geological Survey and Mining Management Agency, Ministry of Economic Affairs, Taipei, Taiwan

(InSAR) before and after the earthquake and estimated fault slip distribution using a half-space dislocation model. We also calculated the pre-seismic surface velocities to examine the interseismic deformation.

2 Data and methods

In this study, we estimated the coseismic displacements using GNSS and InSAR data. In collaboration with GSMMA, we collected and processed the GNSS and InSAR data before and after the earthquake. By using the surface displacements, we employed a simple fault model to estimate the slip distribution and analyzed the pre-seismic deformation near the epicenter.

We computed coseismic displacements from GNSS data by calculating the difference of average coordinates between pre- and post-earthquake. To provide a rapid assessment, we collected raw data from all available continuously-recording GNSS stations across Taiwan three days after the earthquake. Data processing was performed using GipsyX software (Bertiger et al. 2020) with rapid broadcast ephemeris. To have the rapid calculation, the pre-earthquake average coordinates were calculated from January 13, 2025, at 00:00:00 to January 20, 2025, at 16:17:00, while post-earthquake averages were calculated from January 20, 2025, at 16:17:30 to January 23, 2025, at 23:59:30. The coseismic displacements were obtained by subtracting the pre-earthquake from the post-earthquake values.

For InSAR-based coseismic displacements, we applied the differential InSAR (DInSAR) technique using Sentinel-1 single look complex (SLC) images from both ascending and descending tracks, processing with SNAP software (ESA Sentinel Application Platform v10.0.0, http://step.esa.int) developed by the European Satellite Agency (ESA). The ascending images from frames 68 and 74 (path 69) were acquired on January 9 and January 21, 2025, while the descending images from frame 514 (path 105) were collected on January 11 and January 23, 2025. Interferogram generation involved merging the two frames of the ascending images, removing the topographic phase effects, and conducting the multi-looking and Goldstein filtering before phase unwrapping. The same workflow, excluding the merging step, was used for the descending image. The combination of line-of-sights (LOS) displacements from both ascending and descending directions allowed conversion into the east-west and vertical displacement components.

To estimate the pre-seismic surface deformation, we analyzed 10 ascending L-band ALOS-2 SAR images acquired between February 18, 2016, and May 5, 2022. The interferometric processing was performed using ISCE 2 software (Rosen et al. 2012) along with the MintPy software (Yunjun et al. 2019) for the small baseline subset (SBAS) InSAR time series analysis and ionospheric phase removal. Tropospheric phase removal was further addressed using GACOS (Yu et al. 2018), and pixels with coherence below 0.6 were discarded. The LOS deformation rates over the six years were geocoded for the comparison with ground-based GNSS observations.

For fault slip distribution inversion, we constructed two finite fault models with 9×9 grids, which was constrained by the focal mechanism solution from AutoBATS. Therefore, the dip angles of the two possible fault planes were fixed in the model. Moreover, the fault size was designed based on the area with significant surface displacement in the DInSAR results. We considered two fault models: (1) a west-dipping fault plane with a dip angle of 60°, extending 34 km along the strike and 23 km along the dip, and (2) an east-dipping fault plane with a dip angle of 32°, extending 37.8 km along strike and 37.7 km along the dip. The coseismic displacements from GNSS in the three directions and the unwrapped LOS displacements from DInSAR were used as inputs for the inversion. For the InSAR data, we cropped the image around the study area and employed the quadtree downsampling method to decrease the number of observations. We set at least 8×8 quadtree boxes and a threshold of 0.0075 degrees to downsample the InSAR-derived displacements and calculated the mean value in each patch. We reduced the number of pixels from ~4.6 million to 74 pixels in the descending orbit and from ~4.9 million to 55 pixels in the descending orbit. Fault slip was resolved using an elastic half-space dislocation model (Okada 1985) with the non-negative least square (NNLS) method.

3 Results

3.1 Coseismic displacements from InSAR

The InSAR-derived coseismic displacements in the ascending and descending orbits are concentrated in the Nanxi district, southwest of the epicenter, with a radial decrease outward, consistent with the GNSS observations (triangles in Fig. 1c and d). The largest LOS displacements reached 5 cm in the descending track and 7 cm in the ascending track (Fig. 1c and d). The conversion of LOS displacements into the east-west and vertical components revealed minor differences between InSAR and GNSS estimation, suggesting a significant portion of the surface displacements in the north-south direction. Based on the conversion results, the maximum uplift of approximately 4–5 cm was observed in the Nanxi (Fig. 1f), while the most east-west displacements ranged from 3 to 4 cm westward (Fig. 1e).

3.2 Coseismic displacements from GNSS

The coseismic displacements in Fig. 2a and b indicate that the station near the epicenter experienced horizontal displacements of approximately 1–2 cm, with the largest horizontal displacement of 2.3 cm northeastward

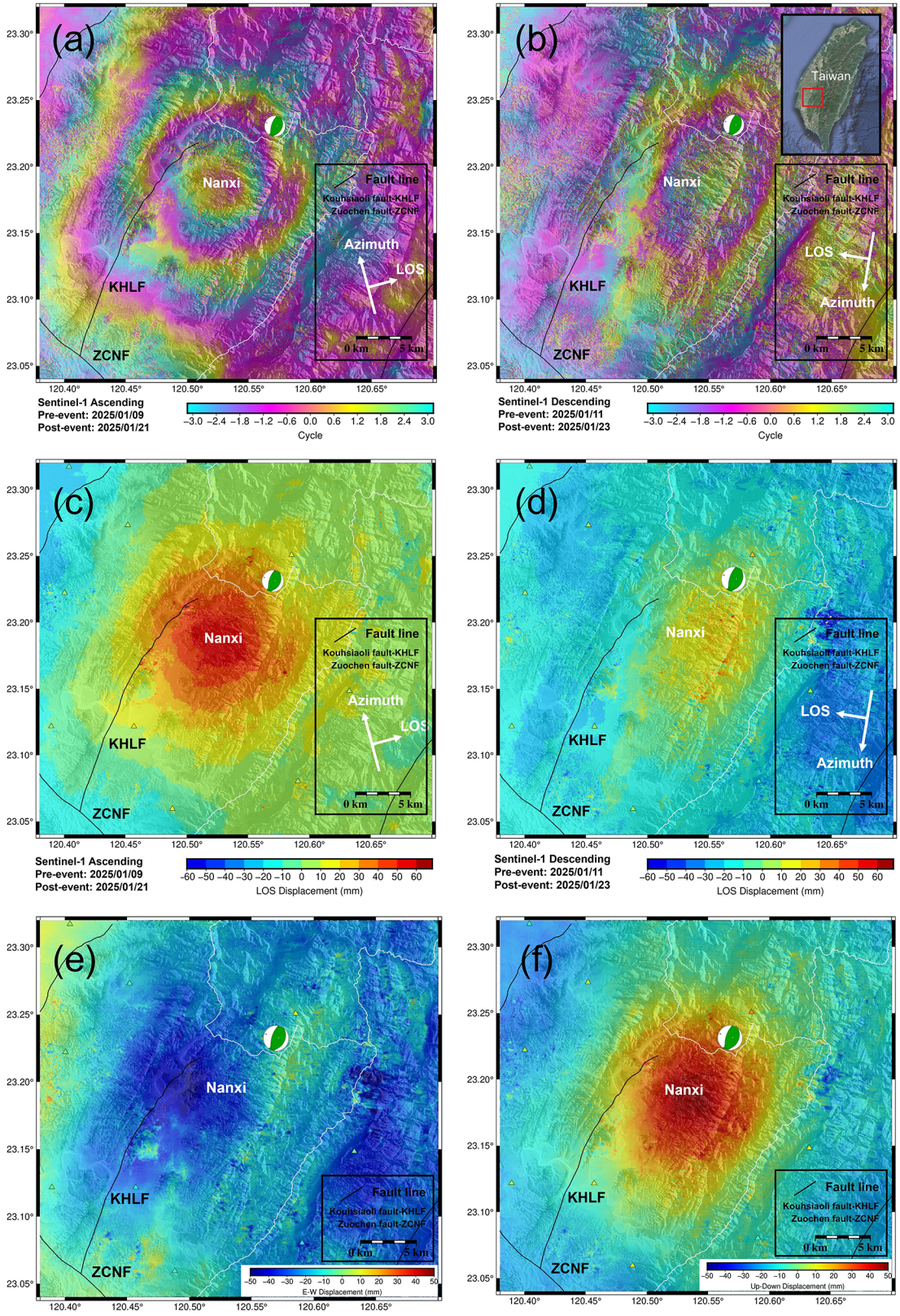

Fig. 1 (**a**) The ascending and (**b**) descending wrapped interferogram. We unwrapped the (**c**) ascending and (**d**) descending results to the LOS displacements. Then, we converted the line-of-sight (LOS) direction displacements to (**e**) east-west and (**f**) Up-down displacements. The most significant displacement area in our results is located in the Nanxi area. Green beach ball represents the focal mechanism of the main shock. The black line represents the GSMMA active fault line. KHLF: Kouhsiaoli fault; ZCNF: Tsochen fault

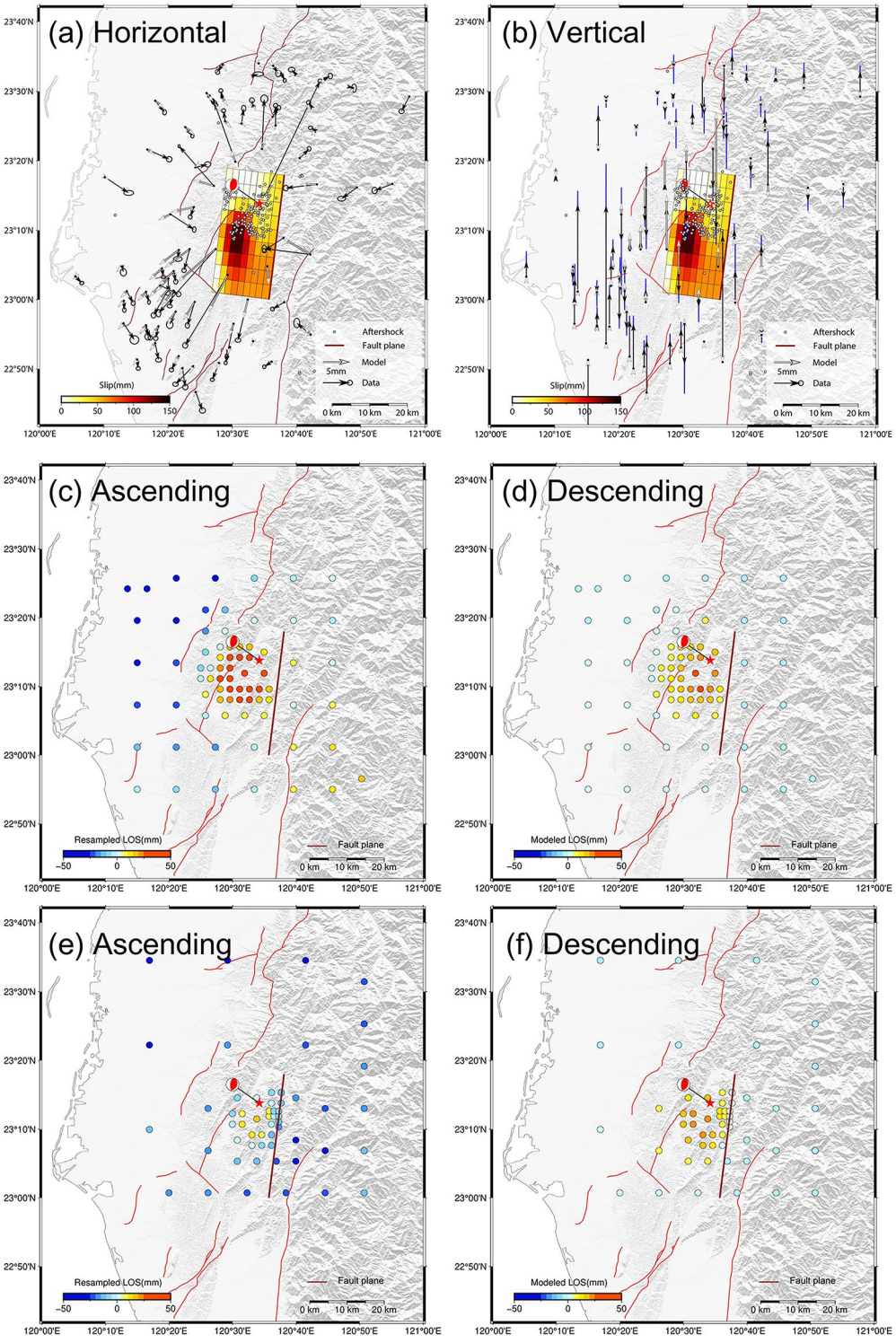

Fig. 2 (**a**) The horizontal and (**b**) vertical direction of GNSS coseismic displacements (black arrows) and modeled data (white arrows). Data uncertainties are black circles and blue bars for the horizontal and vertical directions, respectively. Dark red line represents projected fault line on the surface. Color patches are model fault slip on the west-dipping fault plane. Color dots are LOS displacements with quadtree resampling in the (**c**) ascending and (**d**) descending orbits, and the forward model displacements in the (**e**) ascending and (**f**) descending orbits. The light red line represents the active faults from the Geological Survey and Mining Management Agency

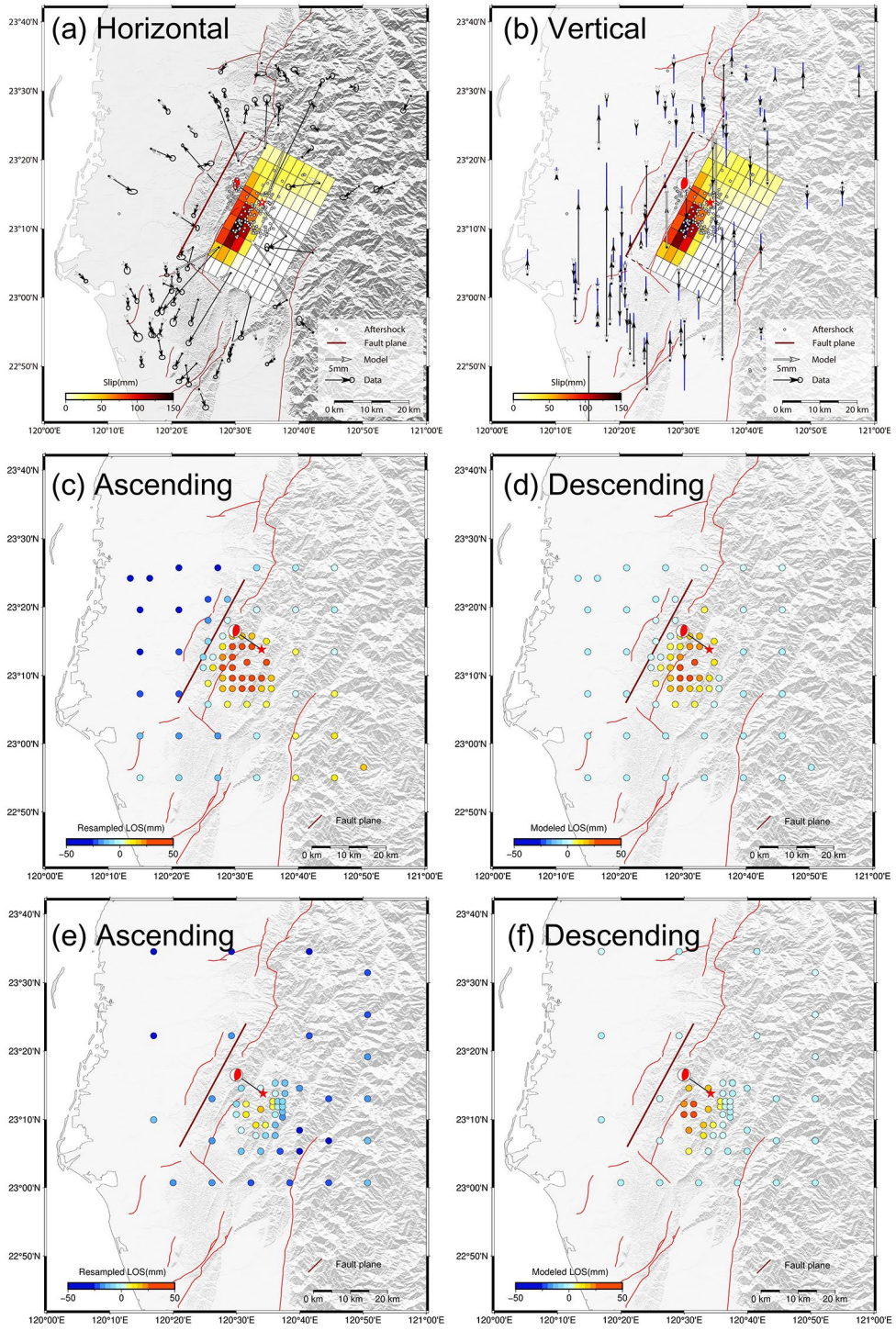

Fig. 3 (**a**) The horizontal and (**b**) vertical direction of GNSS coseismic displacements (black arrows) and modeled data (white arrows). Data uncertainties are black circles and blue bars for the horizontal and vertical directions, respectively. Dark red line represents projected fault line on the surface. Color patches are model fault slip on the east-dipping fault plane. Color dots are LOS displacements with quadtree resampling in the (**c**) ascending and (**d**) descending orbits, and the forward model displacements in the (**e**) ascending and (**f**) descending orbits. The light red line represents the active faults from the Geological Survey and Mining Management Agency

recorded at the TAPU (Dapu) station. Stations farther from the epicenter generally exhibited displacements of less than 1 cm. In the vertical direction, most stations near the epicenter showed an uplift trend, with a maximum vertical displacement of approximately 2.3 cm at TAPU.

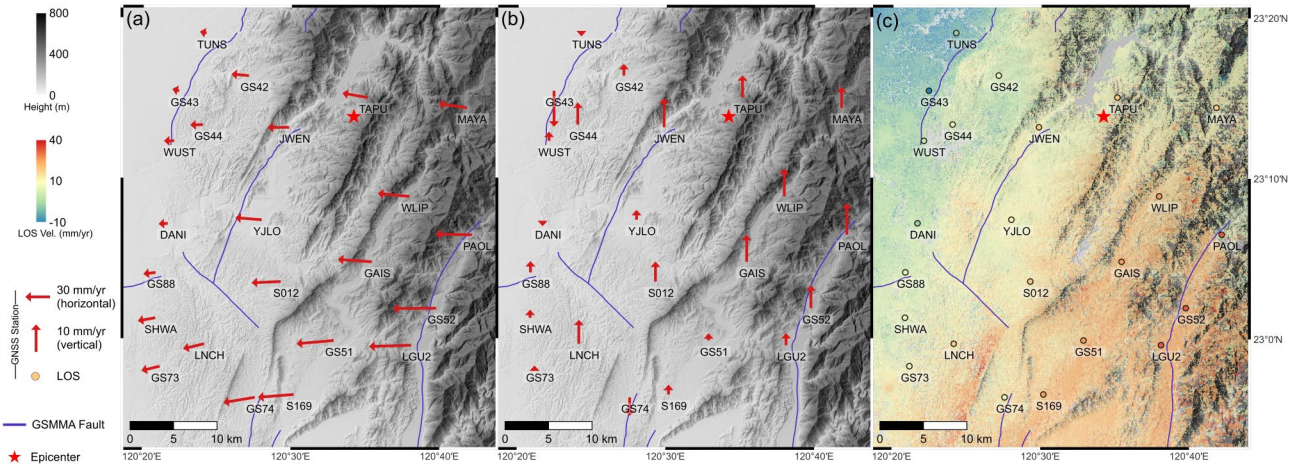

Fig. 4 (**a**) horizontal and (**b**) vertical pre-seismic GNSS velocities from 2017 to 2024 (red arrows); (**c**) Line-of-sight (LOS) velocities derived by ALOS-2 images. Color dots represent the LOS surface velocities converted from the GNSS surface velocities at each GNSS station

3.3 Slip inversion

Our preliminary models provided two sets slip distributions for the two possible fault planes. The model results showed that the west-dipping fault has a good fit to GNSS (Fig. 2a and b) and InSAR data (Fig. 2c and f). The west-dipping fault model indicates that the coseismic slip (Fig. 2a) was primarily concentrated at depths of 7–16 km and extended 15.1 km along the strike, with a maximum slip of approximately 13.5 cm. The primary slip distribution concentrated in the Nanxi District, Tainan City, is consistent with the most affected area observed in GNSS and InSAR data. The modeled seismic movement with 1.102×10^{18}Nm corresponds to an Mw 5.96 earthquake.

For the east-dipping fault plane inversion, the model also exhibited a good fit near the epicenter in GNSS (Fig. 3a and b) and InSAR data (Fig. 3c and f), but the far-field displacements for the east-dipping result presented poor fitting. The model showed that the mainshock slip (Fig. 3a) was primarily concentrated at a depth of 5–12 km and extended 21 km along the strike. The event resulted in approximately 13.9 cm of slip. Similar to the west-dipping result, the primary slip distribution was also located at Nanxi District, Tainan City. The modeled seismic movement with 9.729×10^{17}Nm corresponds to an Mw 5.92 earthquake.

The slip inversion using GNSS and two-directional InSAR data indicates that the west-dipping fault yields a slightly lower root-mean-square (RMS) error of 4.78 mm compared with 4.91 mm for the east-dipping fault. In addition, by comparing aftershocks (Fig. S2), we found that the slip distribution for both fault planes showed a good match with aftershock seismicity.

3.4 Preseismic deformation

To characterize surface deformation before the 2025 Dapu earthquake, we analyzed GNSS data from 24 continuously operated GNSS stations spanning from 2017 to 2024. These stations, distributed over an east-west distance of ~30 km (Fig. 4a), capture a crustal shortening rate exceeding 35 mm/yr. Vertical velocity differences (Fig. 4(b)) between major active faults, such as the Liuchia Fault and Kouhsiaoli Fault, highlight the high deformation rate during this period.

The LOS velocity pattern (Fig. 4(c)) derived from the ALOS-2 images is consistent with the GNSS observations. The LOS velocities across the mainshock area exhibit a few millimeters of shortening but lack a distinct boundary of deformation rate change. This supports the hypothesis that the earthquake was likely triggered by a deeper fault and is not associated with any mapped active faults.

4 Summary

We analyzed geodetic data including GNSS and InSAR, to investigate fault geometry and slip distribution for the 2025 M 6.4 Dapu earthquake in southwestern Taiwan. We present the results of slip inversion for two possible fault planes, which shows fault motion below the detachment with a slightly better fit on the west-dipping fault. GNSS and InSAR data from 2017 to 2024 reveal a high crustal shortening rate (> 35 mm/yr) near the main active faults but no significant velocity discontinuity near the epicenter. This suggests that the earthquake was likely triggered by a buried fault at depth and not associated with any mapped active faults. These findings improve our understanding of subsurface fault structures in southwestern Taiwan and underscore the importance of integrating geodetic data for refining seismic hazard assessments in the region.

Supplementary Information

The online version contains supplementary material available at https://doi.org/10.1007/s44195-025-00090-0.

Supplementary Material 1

Supplementary Material 2

Acknowledgements

We are grateful to the AutoBATS team for providing the seismic solution, the National Land Surveying and Mapping Center, the Ministry of the Interior, the Central Weather Agency, the Geological Survey and Mining Management Agency, the Water Resources Agency, and the Academic Sinica for providing GNSS data. Thanks to the European Space Agency (ESA) for SNAP software and for providing the Sentinel-1 radar images. Special thanks to the Japan Aerospace Exploration Agency (JAXA) for providing the ALOS radar images. We also thank ISCE software, which is funded under the NASA-ISRO SAR (NISAR) project, and the General Mapping Tools (GMT) for methodological support. This study is supported by the National Science and Technology Council with the funding number of 111-2628-M-002-006-MY3.

Author contributions

Conceptualization: [Ray Y. Chuang]; Methodology: [Ray Y. Chuang, Wu-Lung Chang], Formal analysis and investigation: [Zixin Lee, I-Ting Wang, Lishiue Chen, Chi-Yu Chiu]; Visualization: [Zixin Lee, I-Ting Wang, Lishiue Chen]; Writing - original draft preparation: [Zixin Lee, I-Ting Wang, Lishiue Chen, Sheng-Wei Guo]; Writing - review and editing: [Ray Y. Chuang]; Funding acquisition: [Ray Y. Chuang], Resources: [Kuo-En Ching, Chien-Liang Chen], Supervision: [Ray Y. Chuang]. All authors read and approved the final manuscript.

Data availability

The data of this study is available on Figshare: https://doi.org/10.6084/m9.figshare.28521212.

Declarations

Competing interests

The authors declare no competing interests.

Received: 20 February 2025 / Accepted: 8 March 2025
Published online: 02 April 2025

References

Bertiger W, Bar-Sever Y, Dorsey A, Haines B, Harvey N, Hemberger D, Heflin M, Lu W, Miller M, Moore AW, Murphy D, Ries P, Romans L, Sibois A, Sibthorpe A, Szilagyi B, Vallisneri M, Willis P (2020) GipsyX/RTGx, a new tool set for space geodetic operations and research. Adv Space Res 66:469–489. https://doi.org/10.1016/j.asr.2020.04.015

Jian P-R, Tseng T-L, Liang W-T, Huang P-H (2018) A new automatic full waveform regional moment tensor inversion algorithm and its applications in the Taiwan area. Bull Seismol Soc Am 108(2):573–587. https://doi.org/10.1785/0120170231

Le Béon M, Chen C-C, Huang W-J, Ching K-E, Shih J-W, Tseng Y-C, Chiou Y-W, Liu Y-C, Hsieh M-L, Pathier E, Lu C-H, Fruneau B (2024) Aseismic deformation within fold-and-thrust belts: example from the Tsengwen river section of Southwest Taiwan. Geoscience Lett 11:57. https://doi.org/10.1186/s40562-024-00373-3

Lin C-W, Chen W-S (2016) Taiwan Geological Map. https://www.researchgate.net/publication/329415855_Geologic_Map_of_Taiwan

Mouthereau F, Lacombe O, Deffontaines B, Anglier J, Brusset S (2001) Deformation history of the Southwestern Taiwan foreland thrust belt: insights from tectono-sedimentary analyses and balanced cross-sections. Tectonophysics 333(1–2):293–322. https://doi.org/10.1016/S0040-1951(00)00280-8

Okada Y (1985) Surface deformation due to shear and tensile faults in a half-space. Bull Seismol Soc Am 75(4):1135–1154. https://doi.org/10.1785/BSSA0750041135

Ou Y-C, Wu C-L, Chai J-F, Yao G-C (2025) 2025-01-21 Chiayi earthquake report(Version 2.0). National Center for Research on Earthquake Engineering. https://go.ncree.org/eq250121/ (in Chinese)

Rosen PA, Gurrola E, Sacco GF, Zebker H (2012) The InSAR scientific computing environment. In EUSAR 2012; 9th European conference on synthetic aperture radar (pp. 730–733). VDE

The authors declare no competing interests

Wu YM, Lin YH, Yang BM, Ke SS (2025) Performance of the P-Alert real-time shakemaps system and onsite warning during the 2025 ML 6.4 Dapu earthquake. Terr Atmospheric Ocean Sci. https://doi.org/10.1007/s44195-025-00086-w

Yang KM, Huang ST, Wu JC, Ting HH, Mei WW (2010) Review and new insights on foreland tectonics in Western Taiwan. Int Geol Rev 48:910–941

Yu C, Li Z, Penna NT, Crippa P (2018) Generic atmospheric correction model for interferometric synthetic aperture radar observations. J Geophys Research: Solid Earth 123(10):9202–9222

Yunjun Z, Fattahi H, Amelung F (2019) Small baseline InSAR time series analysis: unwrapping error correction and noise reduction. Comput Geosci 133:104331

Publisher's note